Critical design load case fatigue and ultimate failure simulation for a 10-m H-type vertical-axis wind turbine

Journal of Physics: Conference Series **2767** (2024) 072025 doi:10.1088/1742-6596/2767/7/072025

Critical design load case fatigue and ultimate failure simulation for a 10-m H-type vertical-axis wind turbine

[1]**K R Moore,** [2]**I D Brownstein,** [3]**H K Ross**

[1]Sandia National Laboratories, Albuquerque, NM, USA
[2]XFlow Energy Corporation, Seattle, WA, USA
[3]National Renewable Energy Laboratory, Golden, CO, USA

E-mail: kevmoor@sandia.gov

Abstract. While previous studies investigating critical vertical-axis wind turbine (VAWT) design load cases have focused on large and relatively flexible Darrieus designs, the bulk of current commercial products seeking certification fall in the relatively small, stiff, H-type configuration. Understanding the critical design load case impacts for both fatigue and ultimate failure for this size and type of VAWT is imperative for certification and to help break the cycle of historical VAWT failures. A reevaluation of each of the design load cases specified in IEC 61400-1 using the Offshore Wind ENergy Simulator (OWENS) validated aero-servo-elastic software is conducted for both fatigue and ultimate failure contributions. Several design load cases previously thought negligible may have high enough fatigue damage rates for H-VAWTs to warrant more careful consideration; these cases include parked, extreme wind shear, and direction change with gust. Additionally, full operation stop-start-stop cycles, which historically have not been a part of the standards, may contribute fatigue damage similar to other normal design load cases. In light of these potentially critical conditions, and the sizes of many of the current H-VAWT designs falling in the IEC 61400-2 small wind turbine standard, the standard may need to be expanded to enable design success of certified H-VAWT systems.

1. Introduction

While drag-based vertical-axis wind turbines (VAWTs) have been around for at least a millennium [1], lift-based VAWTs are a relatively recent development of the past century [2]. Their highly cyclical loading poses a challenge for design and has led to several historical failures. Perhaps most notably, beginning in the 1970s, Sandia National Laboratories produced several experimental turbines [3, 4, 5, 6] that culminated in the commercialized FloWind product [7]. However, FloWind turbines had several notable cost-cutting design changes that, in combination with limited understanding of fatigue at the time [8], led to the majority of the turbines failing prematurely during the 1990s.

More recently, interest has resurged for VAWTs for certain applications, including distributed power production, offshore power production, and wind farm densification. The archetype may also be better suited for highly turbulent urban environments [9]. The cross-flow nature of the wake dissipates significantly faster than horizontal-axis wind turbine wakes [10]. Entrainment of above-farm momentum can be done with simple design changes like static pitch offset [11]. These effects, including beneficial interference [12], give promise for farm densification. For offshore wind turbines, the lower center of gravity, easy drivetrain access, and fewer active components offer advantages if these designs are placed on floating platforms in deep water [13].

A previous study [14] examined the fatigue and ultimate failure characteristics of a relatively large (5-MW) freestanding and aeroelastically soft Darrieus (curved blade typically in troposkein shape) turbine with no struts. While there are very limited numbers of commercial designs matching this configuration, there are many relatively small, stiff, H-VAWT-type designs (straight blades with struts typically in the shape of the letter H)[1] that are currently working toward certification. As of the writing of this paper, a lack of understanding of the critical design load cases for turbines within this type and size has been noted. While a logical extrapolation of the critical cases may be adequate for academic purposes, a more thorough investigation is

[1] xflowenergy.com, acceleratewind.com, windharvest.com, orpc.co, seatwirl.com, all accessed March 19, 2024

necessary to set these industry players up for success and enable the successful realization of the many benefits VAWTs have to offer.

1.1. Offshore Wind Energy Simulator

The Offshore Wind Energy Simulator (OWENS) was originally developed for VAWTs in 2013 [15], and its models, numerical methods, and architecture have since been significantly improved. The code is an ontology, or glue code, which pulls together preprocessing [16], aerodynamic modules (including double-multiple streamtube and actuator cylinder models modified for unsteady 3D deforming turbines [17] and a free vortex wake method, all including u, v, w inflow turbulence [18]), multi-body structural modules (including linear and nonlinear geometrically exact beam theory [19] and Timoshenko reduced order, linear, and nonlinear models [15]), hydrodynamic modules [20], and postprocessing for fatigue and ultimate failure using classical laminate theory [21]. It uses various coupling, interpolation, meshing, and time-stepping schemes, including generalized torque, aerodynamic, and direct mesh control schemes to enable a wide variety of both axial-flow and cross-flow designs. It has been previously aeroelastically validated for an aluminum Darrieus turbine at the 500-kW scale [22].

1.2. Paper Outline

First, the turbine simulation setup is given. Second, a comparison to currently available data is given. Third, each of the design load cases (DLCs) in IEC 61400-1 [23] is summarized, and the relative contributions for fatigue and ultimate failure are discussed. Finally, the paper is summarized and future work identified.

2. Turbine Simulation Setup

The turbine simulated closely matches the design of the XFlow Energy Co. 10.5-m diameter turbine depicted in Fig. 1a. The simulation has been simplified and generalized compared to the physical turbine to protect the proprietary details of the official design. An attempt to preserve adequate detail to reproduce the results is presented here.

(a) XFlow Energy Co. 10-m turbine showing configuration and overall geometry.

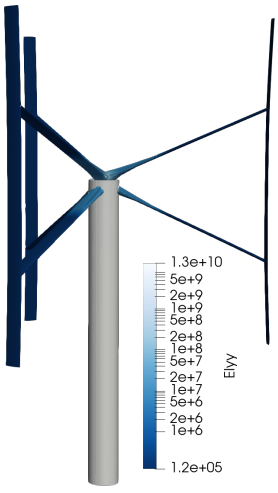

(b) Sample simulated turbine, showing flapwise bending stiffness and sample deflections under normal operation.

Figure 1: Sample experimental turbine and generalized simulation used for this study.

The blades are modeled as constant 0.5-m chord NACA 0018 cross-section pultrusions of standard glass fiber composite. The struts employ the cross section at the tip and gradually taper to a steel-reinforced root. The blade and strut sectional properties were calculated using PreComp[16], a classical laminate theory with a shear flow approach. Without including the very specific design geometry, thicknesses, and material properties due to the pultrusion dependency on pressure and mold shape, we were able to get sectional properties adequate to enable this study. Table 1 shows the used flapwise and chordwise bending sectional properties as a sample, while the simulation additionally calculates all of the properties necessary for the 6 degree-of-freedom nonlinear Timoshenko beam model used.

Table 1: Blade Section Bending Stiffness in N-m^2

	OWENS	Xflow Design
EI Flap Pultrusion	1.21e5	1.26e5
EI Lag Pultrusion	2.87e6	2.10e6
EI Flap Strut Root	4.23e6	6.18e6
EI Lag Strut Root	1.60e7	3.00e6

Figure 1b gives a visual representation of the simulated turbine. The figure includes sample deflections under normal operation and is overlaid with the flapwise bending stiffness showing the taper from hub to blades. Because the selected beam model requires a collection of joined 1D arrays of elements, a rigid hub is not modeled. Instead, past the mounting point, the struts are modeled as a taper into a circular cross section and added steel such that the hub portions are at least 10x stiffer than at the mounting location.

The struts are at approximately 25 degrees and are mounted to the blades with simple pin joints, allowing the moment to pass in the flapwise direction. For this study, the tower was simply modeled as a short and stiff 10-m monopole with a fixed bottom to enable the focus to remain on the rotor.

Simulations conformed to the IEC 61400-1 standard which covers a wide range of cases including startup, normal operation, and shutdown, with varying inflow conditions ranging from gusts, direction change, shear, and turbulence. Any simplifications made attempt to err on the conservative side. The control for normal operation was accomplished using a proportional-integral controller that actively tracks the peak coefficient of performance until the upper RPM limit is reached. For freewheeling conditions (the worst-case fault), the generator torque was simply set to zero. For startup, a prescribed rotor speed sequence was used that took the turbine from standstill to 40 RPM in 30 s. Shutdown was controlled similarly, but in reverse, and emergency shutdown was done similarly, but in 5 s. Normal parked conditions were simulated with the rotor spinning very slowly to capture all angles.

A Class 1, Category A site with an average speed of 10.0 m/s was used with air characteristics matching the winter test conditions at the Spanish Fork, Utah, test site. For all DLCs, the inflow conditions were made to match the standard. The OpenFAST TurbSim model was used to generate the turbulent flow fields at 20 Hz with 26×38 horizontal and vertical discretizations sized to cover the turbine with 25% oversizing. Regarding fault conditions, worst-case control failure of all types for this turbine results in a freewheeling condition. This means that DLCs with the same inflow conditions but specifying different types of faults can be combined.

The OWENS modified double-multiple streamtube aerodynamic model with Boeing-Vertol dynamic stall was used with 24 vertical slices and 30 azimuthal discretizations. Note that the effects of the lifting struts were not captured. These loads were coupled with a Timoshenko multi-body finite element beam model using 10 elements for the tower, 10 elements for each

strut, and 20 elements for each blade. This coupling was run with a time step of 0.01 s with full two-way aeroelastic coupling to capture the expected range of frequencies.

2.1. Dynamic Torque Comparison

Because the software was previously aeroelastically validated [22], and available data were limited due to the current status of the turbine's test campaign, we needed a comparison to increase our confidence in the as-modeled turbine. Partially redacted experimental power performance data are available for the turbine and are shown in Figure 2.

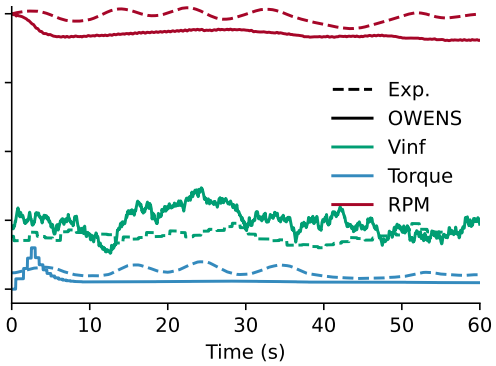

Figure 2: Aeroelastically two-way coupled simulation versus experimental results for DLC 1.1 at nominal 8 m/s. Values redacted due to the preliminary nature of the commercial design.

This case shows a snapshot of the aeroelastically two-way coupled simulation (OWENS) with full-field turbulent inflow matching DLC 1.1 at 8.0 m/s nominal inflow (Vinf), compared against the experimental values for similar conditions (Exp.). Note the simulation startup peak in torque, which was removed (first 10 s) for all simulations except turbine startup cases. While significant uncertainty remains due to the simulation being a generalized approximation of the design, its value for relative comparison between the DLCs seems reasonable, as shown in this power performance comparison.

3. Design Load Case Sweep Setup

While the modeled turbine falls under the small wind turbine standard, IEC 61400-2 [24], the broader set of DLCs in IEC 61400-1 [23] better fulfill this study's goals. Each case is accounted for, except for fault cases that overlap as described previously, and DLC 8.1 where the transport, assembly, and maintenance loads have yet to be defined. Additionally, the standard specifies fatigue or ultimate failure on a case-by-case basis, but we calculate the damage rate and safety factors for every case.

Table 2 gives the breakdown of the Class 1 distribution of fatigue hours in 20 years for each of the used wind speed bins. For the simplicity of comparison, a sparse number of wind speeds were simulated, and 1% of the time in each wind speed bin is spent in startup and 1% of each in shutdown. This gives a slight excess of 20 years, but simplifies the calculations and remains conservative. The 1% startup assumption allows for 2–3 starts and stops in a day, which is used for the stop-start-stop fatigue calculation described in later paragraphs.

For simplification, the location of interest for ultimate failure for the blade is at the strut connection point outer surface in the spar cap. For the strut, it is at the root lower surface in the transition from the fore-panel to the forward shear web. Both of these locations are in compression for all cases, except during the parked conditions. For fatigue loading, the same positions were used, but on the tension side and in the aft panel. These locations are nearly

Table 2: Used wind speed probability distribution for class 1, category A with a mean speed of 10.0 m/s. Note startup and shutdown cases used 1% of each applicable bin's hours for simplicity.

Wind Range	% Time	Hours in 20 years
0–3 m/s	44%	78,043
3–8 m/s	35%	60,831
8–13 m/s	13%	22,791
13–18 m/s	5%	8,538
>18 m/s	3%	5,115

always the highest stress points on the strut and blade, with the occasional exception that the alternate side of the blade/strut has a slightly higher stress. Other simplifications include using only alternating loads with no mean correction factor for fatigue, S-N curves approximated as a basic linear curve fitted with the tensile failure strength at 1 cycle and 25% of the failure strength at 10^8 cycles [25], and the highest wind speed for a bin was used to represent the fatigue damage of that bin. Also, no material knockdown or safety factors were used, so the results show the directly calculated safety factors and fatigue, enabling readers to evaluate the results with different knockdown schemes in mind, especially with respect to potential stress concentrations due to possible joining methods.

Low frequency full operating cycle impacts, or stop-start-stop cycles that span DLCs, are not captured by rainflow counting and do not seem to be accounted for in the IEC standard. While these impacts may be negligible for horizontal-axis wind turbines, they are important for rotorcraft design [26] and may be important for VAWT design. This type of analysis is simply the difference between the highest and lowest loads for a full operation cycle, applied to the fatigue calculations and scaled by the number of lifetime stop-start-stop cycles.

4. Design Load Case Results Discussion

Table 3 provides the results for each of the DLCs and includes the calculated fatigue damage rate for *all* cases in order to reassess the potential impact. Regarding the absolute value of the shown outputs, it is important to reiterate that no material knockdown factors or load safety factors were applied. Additionally, the strut design was intended to be overbuilt to allow for realistic stress concentrations for fastening methods such as bolts and welds, which have been a leading cause of historical VAWT failures. Cases for which fatigue accumulation is not calculated do not have the total damage shown. The time distribution of the normal cases is as previously described, and each major operating condition is discussed below.

4.1. Power Production

Similar to previous studies, damage rate and peak loading follow the wind speed as opposed to peaking at rated speed. Extreme turbulence has a significant impact at lower wind speeds, and high wind speeds near the assumed 18.0 m/s cutout speed see nearly 2 orders of magnitude increase in damage rate for the blade. The ultimate safety factor for this case is also one of the lowest in the blade, but not for the strut. Figure 3 shows a comparison of normal and extreme turbulence effects. The same turbulence seed was used, so the general variations at the hub location are similar. In the full 3D flow field, the variations of the turbulent flow structures are increased substantially, thus giving rise to the increased damage and decreased factor of safety. For sites with significant high-speed turbulence (such as in cities), a turbine like this may need to be derated or include advanced controls to estimate turbulence intensity and control accordingly.

Table 3: IEC 61400-1 DLCs and blade (Bld.) and strut (St.) associated maximum fatigue damage (Dmg.) and minimum ultimate safety factors (Ult. SF).

DLC Description	Wind (m/s)	Dmg./Hr		Dmg.		Ult. SF	
		Bld.	St.	Bld.	St.	Bld.	St.
1.1, 1.2, Power Production	8.0	3.69E-12	4.41E-15	2.25E-07	2.68E-10	5.05	25.07
Normal Turbulence	13.0	1.13E-11	3.98E-15	2.57E-07	9.07E-11	4.43	22.71
	18.0	5.95E-11	8.31E-15	5.08E-07	7.09E-11	3.93	18.85
1.3, Power Production	8.0	6.55E-12	4.05E-15			4.81	22.59
Extreme Turbulence	13.0	3.22E-11	5.93E-15			4.10	19.41
	18.0	1.05E-09	1.20E-14			3.24	15.46
1.4, Power Production	9.0	1.23E-11	7.46E-15			4.71	18.78
Direction Change, Gust	13.0	1.75E-11	6.68E-14			4.73	11.11
1.5, Power Production	8.0	1.73E-12	2.76E-15			5.23	30.49
Extreme Shear	13.0	3.44E-12	3.92E-15			4.83	26.51
	18.0	2.15E-11	7.13E-15			4.14	20.06
2.1, 2.2, 2.4,	8.0	1.78E-12	4.27E-15	1.08E-08	2.60E-11	5.07	25.71
Power Production	13.0	3.86E-11	8.41E-15	8.81E-08	1.92E-11	4.03	17.06
With Fault	18.0	2.99E-10	9.16E-15	2.56E-07	7.82E-12	3.44	16.69
2.3, Power Production	9.0	4.06E-11	4.58E-15			3.93	21.77
Gust with Fault	13.0	2.11E-10	7.47E-15			3.39	17.40
	18.0	4.49E-10	1.87E-14			3.11	13.52
3.1, Startup	8.0	2.30E-12	3.96E-15	1.40E-08	2.41E-11	5.11	26.77
Normal	13.0	3.95E-12	3.02E-15	8.99E-09	6.88E-12	4.99	31.24
	18.0	8.35E-12	3.24E-15	7.13E-09	2.76E-12	4.70	31.38
3.2, Startup	5.0	2.72E-12	3.13E-15			5.07	27.18
with Gust	9.0	3.44E-12	2.58E-15			5.10	29.56
	13.0	6.30E-12	2.67E-15			5.02	32.57
	18.0	1.95E-11	4.99E-15			4.59	28.69
3.3, Startup	5.0	3.85E-12	6.43E-14			5.28	9.97
Direction Change, Gust	9.0	3.44E-12	3.46E-14			5.26	11.51
	13.0	8.22E-12	2.97E-13			5.16	7.89
	18.0	1.06E-10	1.63E-12			4.64	8.64
4.1, Shutdown	8.0	1.75E-11	5.04E-15	1.07E-07	3.07E-11	4.00	21.56
Normal	13.0	4.68E-11	8.12E-15	1.07E-07	1.85E-11	3.87	17.95
	18.0	3.24E-10	9.00E-15	2.76E-07	7.69E-12	3.49	17.99
4.2, Shutdown	9.0	1.59E-11	6.08E-15			3.97	20.78
with Gust	13.0	7.47E-11	8.93E-15			3.72	18.74
	18.0	2.45E-10	7.04E-15			3.30	17.80
5.1, Emergency	9.0	1.15E-10	5.25E-15			3.51	18.43
Shutdown	13.0	4.27E-10	7.17E-15			3.34	15.41
	18.0	2.02E-09	2.06E-14			2.97	12.29
6.1, Parked, 50yr	50.0	6.72E-09	1.04E-13			4.66	13.63
6.2, Parked, Fault	50.0	5.48E-03	1.33E-07			1.75	1.88
6.3, 7.1, Parked, 1yr	30.0	9.19E-12	9.63E-16			7.64	25.77
6.4, Parked, Normal	35.0	1.92E-11	3.93E-15	1.64E-07	3.36E-11	7.20	23.88
20 Year Damage				2.03E-06	6.07E-10		
Description	Cycles	Dmg./Cyc		Dmg.			
		Bld.	St.	Bld.	St.		
Stop-Start-Stop	21900	1.11E-13	9.82e-20	2.44e-9	2.15e-15		

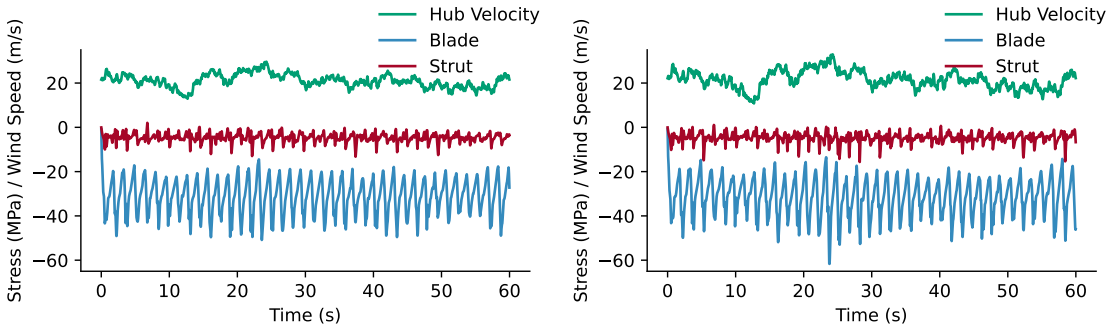

(a) DLC 1.1 normal turbulence.

(b) DLC 1.3 extreme turbulence.

Figure 3: Power production at nominal 18 m/s showing hub wind speed versus the sampled blade and the principal material stress for the strut positions. Extreme turbulence increases the peaks of the loads and the frequency of those peaks.

Cases 1.4 and 2.3 include gust impacts. They experience greater loads at lower wind speeds due to the simulated gust being of the same magnitude regardless of nominal speed. Additionally, the gust length for DLC 1.4 is for a longer effective duration than the extreme operating gust in DLC 2.3, which has a role in the relative loading between the two. However, DLC 2.3 also includes fault, which for this system is a freewheeling turbine. At higher wind speeds, the turbine accelerates quickly to a high rotational rate before max RPM and a fail-safe system can be applied. Extreme shear, especially at higher wind speeds, also produces significant loads for the blades. In part, this may be because it violates a fundamental design assumption of blade balance for this type of turbine. For a Darrieus configuration, shear may be less impactful, as the design already includes large variations in loads along the blade due to varying radius and, in many cases, chord.

4.2. Startup

Startup was originally simulated using the normal operation controller, but the turbine was taking several minutes of simulation time to get up to speed and producing a negligible damage rate. A more conservative 30 s forced RPM from 0 to the design 40 RPM was used. Despite this, the damage rate and overall accumulated damage is small relative to power production, but non-negligible. Gust and direction change appear to not increase blade loading appreciably for this case, likely due to the low tip speed ratios and high load fluctuations already present. However, the struts experience a significant increase in loading, which may be due to an unfavorable loading combination and may be the topic of future work to investigate further. A condition could arise where the changing wind speed aligns with the motion of the blade to delay and then elongate and amplify the peak load during dynamic stall, temporally increasing torque substantially by elastic means.

4.3. Shutdown

Shutdown seems to be more impactful than startup and nearly as impactful as power production. Emergency shutdown damage rate increases and safety factors decrease, with the damage accumulation from a high-speed shutdown nearly 10x that of normal shutdown. Due to the high damage rate, a turbine that accumulates enough instances of this condition may quickly build non-negligible damage. Figure 4a shows an example of the emergency shutdown case.

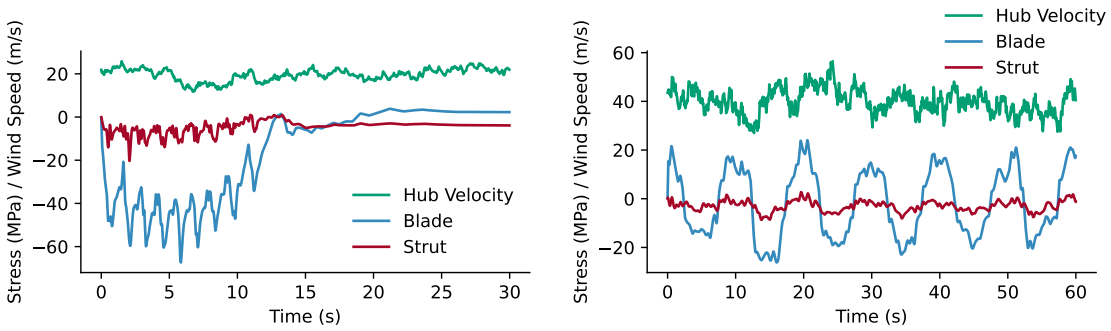

(a) DLC 5.1 emergency shutdown at 18.0 m/s.

(b) DLC 6.4 parked at 35.0 m/s.

Figure 4: Examples of two of the most damaging cases behind normal power production.

4.4. Parked

For the normal parked case, DLC 6.4, the standard specifies 0.7 times the reference speed (50 m/s for Class 1), corresponding to the relatively high wind speed of 35 m/s (see Fig. 4b). With this high specified speed, only the high-speed distribution of 3% time was applied, as opposed to additionally including the large amount of time below 3 m/s. Despite this relatively small amount of time, the accumulated fatigue is on the same order of magnitude as the startup cases and nearly that of the shutdown cases. The double-multiple streamtube model does not account for higher-order effects such as vortex shedding at high angles of attack. The method does use Viterna extrapolation to 360° [27] and so accounts for the first order effects. However, should there be an unaccounted forcing frequency that excites a blade mode, the damage for this case could *substantially* increase. Additionally, the 50-year extreme wind case with fault allowing the turbine to begin to spin up out of idle may be the driving load case for failure. The authors of [14] also noted the potential of the parked cases to be critical but did not go into significant detail, as their design was not stable for their simulated parked conditions. The design presented here is significantly stiffer and was stable, but still shows relatively high loading and fatigue accumulation, suggesting higher-fidelity investigation and detail may be warranted for the parked cases.

4.5. Stop-Start-Stop

The stop-start-stop cycles' maximum stress for the blade was found to be 78.2 MPa during shutdown, and the minimum stress was −4.19 MPa during startup. For the strut, the maximum was during startup at 9.92 MPa, and the minimum was during shutdown at −0.15 MPa. The resulting damage is on the same order of magnitude as startup for the blades and less pronounced for the struts. Designs that are larger and more flexible may see this increase.

5. Conclusions

Based on the results and discussion, the following DLCs are ranked in order as likely contributors to the critical design of the size and type of VAWT investigated.

For fatigue:

- Parked, noting high angles of attack uncertainty
- Power production, noting the significance of increasing turbulence
- Direction-change cases, which may need further investigation

- Shutdown, noting that emergency shutdown can be 10x as damaging
- Stop-start-stop full operation cycles

For ultimate failure:

- Parked 50-year extreme wind with fault
- Emergency shutdown
- Direction-change cases
- Extreme turbulence

One should also take note that many of the cases are relatively close to one another in damage rates and in peak stress. Small changes in design may shift the ordering of the critical DLCs, which would make certifying a design a thorough endeavor. Additionally, the loads investigated here are for the bulk structures, while historical failures have been in stress or load concentration areas such as welds, bolts, and bearings. Additional care should be made for stages of detailed design where bulk loads from aeroelastic modeling could be used as inputs.

6. Future Work

With the potential confirmation that the parked cases are a main driving factor for both ultimate and fatigue loading for a non-blade-pitching VAWT regardless of type, it is recommended that improvements in the mid- to low-fidelity modeling capabilities for very high angles of attack be made. Potential candidates of research may include incorporating a dynamic oscillator model or more comprehensive machine learning models trained on high-fidelity unsteady aerodynamics to account for unsteady vortex shedding at high angles of attack. Additionally, due to the cyclical loading aligned with the tower, the tower and cable dynamics should be considered for future research.

7. Acknowledgements

Sandia National Laboratories is a multi-mission laboratory managed and operated by National Technology & Engineering Solutions of Sandia, LLC (NTESS), a wholly owned subsidiary of Honeywell International Inc., for the U.S. Department of Energy's National Nuclear Security Administration (DOE/NNSA) under contract DE-NA0003525. This written work is authored by an employee of NTESS. The employee, not NTESS, owns the right, title and interest in and to the written work and is responsible for its contents. Any subjective views or opinions that might be expressed in the written work do not necessarily represent the views of the U.S. Government. The publisher acknowledges that the U.S. Government retains a non-exclusive, paid-up, irrevocable, world-wide license to publish or reproduce the published form of this written work or allow others to do so, for U.S. Government purposes. The DOE will provide public access to results of federally sponsored research in accordance with the DOE Public Access Plan.

This work was authored in part by the National Renewable Energy Laboratory, operated by Alliance for Sustainable Energy, LLC, for the U.S. Department of Energy (DOE) under Contract No. DE-AC36-08GO28308. Funding provided by the U.S. Department of Energy Office of Energy Efficiency and Renewable Energy Wind Energy Technologies Office.

References

[1] D G Shepherd. Historical development of the windmill. 12 1990.
[2] G. J. M. Darrieus. Turbine having its rotating shaft transverse to the flow of the current. U.S. Patent, Oct 1926. US1835018A.
[3] B F Blackwell, R E Sheldahl, and L V Feltz. Wind tunnel performance data for the darrieus wind turbine with naca 0012 blades. 5 1976.
[4] Robert E. Sheldahl, Paul C. Klimas, and Louis V. Feltz. Aerodynamic performance of a 5-metre-diameter darrieus turbine with extruded aluminum naca-0015 blades. Technical Report SAND-80-0179, Sandia National Laboratories, 3 1980.
[5] Mark H. Worstell. Aerodynamic performance of the doe/sandia 17-m-diameter vertical-axis wind turbine. *Journal of Energy*, 5(1):39–42, 1981.
[6] T D Ashwill. Measured data for the sandia 34-meter vertical axis wind turbine. 7 1992. SAND-91-2228.
[7] Alcoa. Design and fabrication of a low-cost darrieus vertical-axis wind-turbine system, phase ii. volume 2. final technical report. Technical report, 3 1983.
[8] PF Packman. Aging aircraft and fatigue failure. *J. Air L. & Com.*, 54:965, 1988.
[9] S.J. Kooiman and S.W. Tullis. Response of a vertical axis wind turbine to time varying wind conditions found within the urban environment. *Wind Engineering*, 34(4):389–401, 2010.
[10] Matthieu Boudreau and Guy Dumas. Comparison of the wake recovery of the axial-flow and cross-flow turbine concepts. *Journal of Wind Engineering and Industrial Aerodynamics*, 165:137–152, jun 2017.
[11] Ming Huang, Andrea Sciacchitano, and Carlos Ferreira. On the wake deflection of vertical axis wind turbines by pitched blades. *Wind Energy*, 26(4):365–387, 2023.
[12] Ian D. Brownstein, Nathaniel J. Wei, and John O. Dabiri. Aerodynamically interacting vertical-axis wind turbines: Performance enhancement and three-dimensional flow. *Energies*, 12(14):2724, jul 2019.
[13] Brandon Lee Ennis and D Todd Griffith. System levelized cost of energy analysis for floating offshore vertical-axis wind turbines. Technical report, Sandia National Lab.(SNL-NM), Albuquerque, NM (United States), 2018.
[14] Christos Galinos, Torben J. Larsen, Helge A. Madsen, and Uwe S. Paulsen. Vertical axis wind turbine design load cases investigation and comparison with horizontal axis wind turbine. *Energy Procedia*, 94:319–328, 2016. 13th Deep Sea Offshore Wind R&D Conference, EERA DeepWind'2016.
[15] Brian C. Owens. *Theoretical Developments and Practical Aspects of Dynamic Systems in Wind Energy Applications*. PhD thesis, Texas A&M, 2013.
[16] G. S. Bir. *User's guide to PreComp (Pre-Processor for Computing Composite Blade Properties)*. National Renewable Energy Laboratory, 2006.
[17] Kevin R. Moore and Brandon L. Ennis. Vertical-axis wind turbine steady and unsteady aerodynamics for curved deforming blades. *AIAA Journal*, 60(1):189–196, 2022.
[18] NREL. Openfast. open-source wind turbine simulation tool, available at http://github.com/openfast/openfast, 2022.
[19] Taylor McDonnell and Andrew Ning. Gxbeam: A pure julia implementation of geometrically exact beam theory. *Journal of Open Source Software*, 7(73):3997, May 2022.
[20] Michael C. Devin, Nicole R. Mendoza, Andrew Platt, Kevin Moore, Jason Jonkman, and Brandon L. Ennis. Enabling floating offshore vawt design by coupling owens and openfast. *Energies*, 16(5), 2023.
[21] Andreas Öchsner. *Foundations of classical laminate theory*. Springer, 2021.
[22] K. R. Moore and B. L. Ennis. Aeroelastic validation of the offshore wind energy simulator for vertical-axis wind turbines. *Wind Energy Science Discussions*, 2022:1–28, 2022.
[23] International Electrotechnical Commission et al. Wind turbines-part 1: design requirements. *IEC61400-1*, 2019.
[24] International Electrotechnical Commission et al. Wind turbines - part 2: Small wind turbines. *IEC61400-1*, 2013.
[25] L. Roy Xu and Vikram Bhamidipati. An efficient method to estimate the s-n curves of engineering materials.
[26] Federal Aviation Association. 14 cfr § 27.571 fatigue evaluation of flight structure. Electronic Code of Federal Regulations (e-CFR).
[27] Larry Viterna and David Janetzke. Theoretical and experimental power from large horizontal-axis wind turbines. *NASA Technical Memorandum*, 10 1982.